Author's Accepted Manuscript

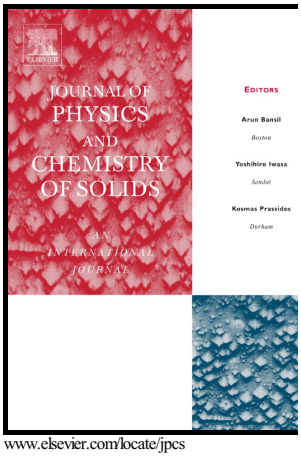

www.elsevier.com/locate/jpcs

Compressibility of orthorhombic perovskites.Compressibility of orthorhombic perovskites. the effect of transition metal Ions (TMI)

Matteo Ardit

PII: S0022-3697(15)30041-X
DOI: http://dx.doi.org/10.1016/j.jpcs.2015.08.010
Reference: PCS7613

To appear in: *Journal of Physical and Chemistry of Solids*

Received date: 1 April 2015
Revised date: 20 July 2015
Accepted date: 17 August 2015

Cite this article as: Matteo Ardit, Compressibility of orthorhombi perovskites.Compressibility of orthorhombic perovskites. the effect of transitio metal Ions (TMI), *Journal of Physical and Chemistry of Solids* http://dx.doi.org/10.1016/j.jpcs.2015.08.010

This is a PDF file of an unedited manuscript that has been accepted fo publication. As a service to our customers we are providing this early version o the manuscript. The manuscript will undergo copyediting, typesetting, an review of the resulting galley proof before it is published in its final citable form Please note that during the production process errors may be discovered whic could affect the content, and all legal disclaimers that apply to the journal pertain

ACCEPTED MANUSCRIPT

Compressibility of orthorhombic perovskites. The effect of Transition Metal Ions (TMI)

Matteo Ardit
Department of Physics and Earth Sciences, University of Ferrara, via Saragat 1, I-44122 Ferrara, Italy
e-mail: rdtmtt@unife.it

Abstract. Interest in perovskites evenly spans Materials Science and Geophysics. Due to their inimitably lattice flexibility enabling small as well as large ions to be accommodated, perovskites have become a base structure for new technological applications. Understanding the mechanisms governing their evolution at non-ambient conditions (such as high-pressure and high-temperature) is fundamentally important both for devising functional materials and in order to provide the most reliable possible deep-Earth model. With particular attention being paid to the chemical nature of the constituent ions, a suite of orthorhombic perovskites has been selected and contrasted using several parameterizations and models. A new perspective on the pressure-induced distortion of orthorhombic perovskite structures has enabled their compressional behaviour to be redefined.

Keywords: A. inorganic compounds; A. oxides ; C. high pressure; D. crystal structure.

Personal Keywords: orthorhombic perovskites; high-pressure; transition metal ions; octahedral tilting; polyhedral compressibility.

Accepted manuscript

1. Introduction

Perovskite compounds, with the general stoichiometry ABX_3, have certainly become one of the most important and highly-studied class of materials. Superconductors [1], non-toxic inorganic pigments [2], sensitizers in dye-sensitized solar cells (DSSCs) [3], and photoluminescent semiconductors [4] are just a few examples which describe the extraordinary flexibility of perovskites in the field of Materials Science.

The archetypal perovskite has a cubic structure (s.g. Pm-3m) with A cations located at the centre of dodecahedral sites defined by a framework of eight corner-sharing BX_6 octahedra [5]. In this ideal case, the A–X/B–X ratio is equal to $\sqrt{2}$, but the lattice can be stressed for most perovskite compounds and the A–X/B–X ratio varies [6]. The degree of distortion from cubic symmetry can be described in terms of octahedral tilting and more distorted polyhedra, and is a function of the chemical nature of A and B cations (i.e. size, valence, electronic configuration, etc.) as well as changes in pressure and temperature conditions. The structural answer to these internal and external stresses is a decrease in symmetry: for instance, to rhombohedral, tetragonal, monoclinic, and more frequently, orthorhombic [e.g. 5,7-9].

As recently emphasized by Duffy [10], perovskites have also received considerable attention in Earth Sciences, since it was discovered that the main minerals in the upper mantle (i.e. olivine, pyroxene, and garnet) undergo a series of phase transitions to the denser $(Mg,Fe)SiO_3$ perovskite structure (s.g. Pbnm), at upper/lower mantle interface pressure and temperature conditions [11,12]. The importance of this mineral further grew in 2004 when it was realized that $(Mg,Fe)SiO_3$ perovskite transforms to a more compact layered atomic arrangement known as post-perovskite (s.g. Cmcm) at core-mantle boundary conditions [13]. The features of this latter phase seem to explain several observed properties in the so called D'' layer [14].

In this exciting context, perovskite oxides have become the subject of many studies devoted to establishing their behaviour at high-pressure. Some of these studies [15-20] have attempted to predict the evolution of these compounds from a common paradigm which enables the pressure-induced evolution of an orthorhombic perovskite to be rationalized in terms of the relative compressibility of its two polyhedra (i.e. AO_{12} dodecahedra and BO_6 octahedra). Specifically, two distinct patterns of compression have been outlined [e.g. 17,21,22]. When AO_{12} dodecahedra are more compressible than BO_6 octahedra, volume reduction will lead to an increase in octahedral tilting (e.g. an extreme case is represented by the rigid-unit model [18]). Conversely, when AO_{12} dodecahedra are less compressible than BO_6 octahedra, the perovskite structure will evolve, decreasing octahedral tilting by raising its symmetry towards the cubic archetype.

ACCEPTED MANUSCRIPT

While this paradigm has long been known, parameterizations and models of perovskite high-pressure behaviour have become more accurate, as have experimental methods, in conjunction with an increase in experimental data.

Besides these considerations, the study of perovskites bearing transition metal ions (TMI, such as Ti, V, Cr, Mn, Fe, Co, Ni, and Cu) has often paved the way to new functional materials. Hundreds of studies have proven the close interplay between external conditions (i.e. high- and low-temperature as well as high-pressure) and the outstanding physical properties (e.g. colossal magnetoresistance, insulation, semiconduction, metallic conduction, diamagnetism, paramagnetism, ferromagnetism, and many others) which perovskites are designed and utilised for [e.g. 23-27]. Moreover, it has been demonstrated that Fe^{3+} spin transition effects can strongly influence the density and compressibility of silicate perovskite at lower mantle depth [28].

Albeit the undisputed importance of TMI-bearing perovskites in both Materials and Earth Sciences, a general view of these compounds with pressure is lacking.

Given that a deep understanding of the relationship between external conditions (such as P and T), structural properties and chemistry of perovskite compounds is essential both to designing a compound with specific properties and to determining its most reliable model at deep-Earth conditions, this contribution is aimed at examining the effects of TMI on the compressibility of orthorhombic perovskites with respect to those "TMI free". The comparison of the various compounds will take place through a brief review of some rationalizations and models proposed in literature as well as using a more recent approach known-as the "polyhedral bond-valence ratio" [29,30].

2. Compound selection

A selection of orthorhombic perovskite oxides with their literature references at ambient and high-pressure conditions has been compiled in Table 1.

Table 1

Code, mineral formula, and references for the selected compounds at both ambient and high-pressure. Alongside the "High-Pressure" column is the maximum pressure reached during high-pressure experiments for each cited work (P_{max}).

	Code	Mineral formula	References		P_{max} (GPa)
			Ambient	High-Pressure	
3:3 TMI	PNM	$Pr_{0.75}Na_{0.25}MnO_3$	[31]	[31]	8.3
	YT	$YTiO_3$	[32]	[33]	30.0
	YC	$YCrO_3$	[34]	[35,36]	60.4
	GF	$GdFeO_3$	[37]	[37]	8.1
	LM	$LaMnO_3$	[38]	[39]	40.0
	GM	$GdMnO_3$	[40]	[41]	63.1
3:3 noTMI	SA	$ScAlO_3$	[42]	[42]	5.2
	GA	$GdAlO_3$	[37]	[37]	8.5
	YA	$YAlO_3$	[43]	[43]	8.8
	NG	$NdGaO_3$	[44]	[44]	8.1
	LG	$LaGaO_3$	[44]	[44]	2.2
2:4	SC	$SrCeO_3$	[45]	[46]	7.9
	CSn	$CaSnO_3$	[47]	[47,48]	6.7, 8.5
	MS	$MgSiO_3$	[49]	[49,50]	15.0, 10.0
	CSi	$CaSiO_3$	[51]	[51]	160
	CT	$CaTiO_3$	[52]	[52,53]	8.1, 9.7
	CG	$CaGeO_3$	[6]	[53]	8.6
	CZ	$CaZrO_3$	[54]	[55]	8.7

In order to make data interpretation as clear and incisive as possible, the selected compounds have been subdivided on the basis of their chemistry. Specifically, three "families" have been identified: 3:3 TMI (i.e. compounds characterized by cations with the same formal valence (i.e. 3+) at both A and B sites, and with octahedra occupied with TMI); 3:3 noTMI (i.e. as per previous compounds but "TMI free"); and 2:4 (i.e. compound characterized by cations with nominal valence 2+ and 4+ at the cubic and octahedral site,

Accepted manuscript

ACCEPTED MANUSCRIPT

respectively). Additionally, data plotted in each figure have been subdivided by different symbols, i.e. diamonds for 3:3 TMI, circles for 3:3 noTMI, and squares for 2:4.

Compounds have been chosen by combining the following criteria: (1) data at both ambient and high-pressure conditions must be available; (2) studies at high-pressure must report unit-cell parameters and isothermal bulk modulus at the least (in the case of multiple reports, priority has been given to studies which report polyhedral compressibility) (3) complete structural details (i.e. unit-cell parameters and refined atomic coordinates) must be available for each compound at ambient conditions.

Table 2

Unit-cell volume, mean polyhedral bond distances, interoctahedral bond angles, and polyhedral volumes for the selected compounds at ambient pressure. Standard deviations are reported in brackets.

	Code	volume (Å^3)	polyhedral bond distances (Å)				octahedral bond angles (°)			polyhedral volumes (Å^3)		
		V	$\langle A–O\rangle^{12}$	$\langle A–O\rangle^{8}$	$\langle A–O\rangle^{4}$	$\langle B–O\rangle$	B–O1–B	B–O2–B	$\langle B–O–B\rangle$	$V(AO_{12})$*	$V(AO_8)$	$V(BO_6)$
3:3 TMI	PNM	227.40(8)	2.733(5)	2.570(5)	3.059(5)	1.956(8)	160.50(60)	157.87(50)	159.13(55)	46.87(5)	25.99(5)	9.98(5)
	YT	231.24(4)	2.806(3)	2.439(3)	3.542(4)	2.044(1)	140.18 (3)	143.58 (2)	141.88 (3)	46.45(3)	24.40(3)	11.36(3)
	YC	218.27(1)	2.738(2)	2.417(2)	3.379(3)	1.984(3)	146.84(18)	145.86(15)	146.35(17)	44.16(3)	23.52(2)	10.40(3)
	GF	230.42(2)	2.782(2)	2.469(2)	3.409(3)	2.015(1)	147.28(10)	146.93(13)	147.10(12)	46.71(2)	24.94(2)	10.89(2)
	LM	243.63(5)	2.809(5)	2.582(5)	3.262(5)	2.012(2)	155.97(70)	155.90(30)	155.94(50)	50.09(5)	27.12(5)	10.82(4)
	GM	231.77(1)	2.810(4)	2.448(4)	3.533(5)	2.028(3)	145.68(30)	145.98(20)	145.83(25)	46.93(4)	24.58(4)	11.02(3)
3:3 noTMI	SA	186.10(3)	2.608(3)	2.273(3)	3.277(4)	1.903(3)	140.85(30)	142.69(20)	141.77(25)	37.35(3)	19.64(3)	9.17(3)
	GA	207.41(1)	2.658(3)	2.456(3)	3.063(3)	1.906(2)	155.98(14)	156.16(18)	156.07(16)	42.63(3)	23.43(3)	9.23(3)
	YA	203.49(1)	2.654(2)	2.402(2)	3.157(3)	1.910(1)	152.46(18)	151.82(10)	152.15(15)	41.59(2)	22.53(2)	9.28(2)
	NG	230.13(1)	2.756(3)	2.527(3)	3.216(3)	1.981(1)	154.34(24)	153.97(20)	154.16(22)	47.16(3)	25.74(3)	10.36(2)
	LG	235.81(2)	2.764(4)	2.611(4)	3.071(4)	1.977(1)	158.07(22)	160.51(20)	159.28(21)	48.65(3)	27.07(3)	10.30(1)
2:4	SC	316.82(2)	3.087(5)	2.752(5)	3.757(5)	2.250(3)	142.80(30)	146.51(25)	144.66(27)	64.07(5)	33.85(5)	15.16(4)
	CSn	246.14(2)	2.836(3)	2.537(3)	3.435(4)	2.056(2)	147.04(23)	147.87(13)	147.45(19)	49.96(2)	26.68(2)	11.58(3)
	MS	162.53(5)	2.474(1)	2.205(1)	3.010(1)	1.793(3)	146.73(20)	147.31(20)	147.02(20)	32.96(5)	17.61(5)	7.68(3)
	CSi	178.30(5)	2.511(5)	2.425(5)	2.684(5)	1.784(3)	167.92(30)	166.53(30)	167.22(30)	37.01(5)	21.16(5)	7.56(4)
	CT	223.91(3)	2.727(5)	2.518(5)	3.144(5)	1.957(2)	156.39(28)	155.32(26)	155.86(27)	45.99(2)	25.23(2)	9.98(2)
	CG	206.36(6)	2.647(4)	2.481(4)	2.979(5)	1.892(3)	160.38(30)	158.96(20)	159.67(25)	42.56(4)	23.69(4)	9.03(4)
	CZ	258.26(2)	2.884(3)	2.572(2)	3.510(3)	2.096(1)	145.76(20)	146.50(20)	146.13(20)	52.30(3)	27.81(3)	12.27(3)

Note: polyhedral volume $V(AO_{12}) = (V / 4) – V(BO_6)$.

Accepted manuscript

ACCEPTED MANUSCRIPT

Table 3
Parameters derived from data at ambient pressure (observed tolerance factor, $^{VIII}t_{obs}$, polyhedral volume ratio, V_A/V_B*, normalized cell distortion factor with pressure, $d_{norm}(P)$, bond valence matching, M_A/M_B, and polyhedral bond-valence sum ratio, $BVsum_{obs}/BVsum_{id}$), and data at high-pressure (unit-cell volume compressibility, K_{T0}, with its first pressure derivative, K', and polyhedral volumes, K_{P0}, as expressed in terms of bulk moduli). Standard deviations are in brackets.

	Code	$^{VIII}t_{obs}$ (eq 1)	V_A/V_B* (eq 2)	$d_{norm}(P)$ (GPa^{-1}) (eq 5)	M_A/M_B (eq 6)	$BVsum_{obs}/BVsum_{id}$	K_{T0} (GPa)	K'	$K_{P0}(A)$ (GPa)	$K_{P0}(B)$ (GPa)
3:3 TMI	PNM	0.929(4)	4.69	0.688	0.86(16)	0.96(4)	157(5)	4.0(1.0)	163(9)	128(8)
	YT	0.844(2)	4.09	0.039	1.05(10)	0.99(1)	163(6)	8.5(1.0)	193(7)	176(6)
	YC	0.861(1)	4.25	0.010	1.18 (9)	1.01(1)	208(1)	3.7(0.1)	202(5)	189(8)
	GF	0.867(1)	4.29	-0.002	1.15 (7)	1.01(1)	182(1)	6.3(0.3)	188(2)	188(10)
	LM	0.907(3)	4.61	-0.070	1.23(15)	1.02(2)	108(2)	8.5(0.4)	145(8)	92(5)
	GM	0.854(3)	4.24	-0.015	1.22(15)	1.03(2)	156(3)	6.5(0.3)	–	–
3:3 noTMI	SA	0.845(2)	4.07	0.382	1.14(13)	0.96(2)	218(1)	4.0(2.0)	220(10)	200(10)
	GA	0.911(1)	4.62	0.009	1.45(11)	1.01(2)	191(1)	5.8(0.3)	204(5)	179(8)
	YA	0.890(1)	4.48	-0.041	1.41 (9)	1.00(1)	192(2)	7.3(0.4)	208(5)	177(6)
	NG	0.902(1)	4.55	-0.097	1.18 (9)	1.00(1)	177(2)	6.7(0.6)	195(4)	162(7)
	LG	0.934(2)	4.72	-0.103	1.23(12)	1.01(2)	172(1)	6.4(fixed)	186(2)	134(5)
2:4	SC	0.865(2)	4.21	0.239	0.56(12)	0.85(2)	110(1)	4.0(fixed)	102(5)	159(7)
	CSn	0.872(1)	4.31	0.148	0.56 (8)	1.00(2)	163(1)	5.6(0.3)	158(2)	195(6)
	MS	0.870(2)	4.29	0.040	0.70 (4)	1.03(1)	253(1)	4.0(fixed)	270(20)	310(20)
	CSi	0.962(3)	4.89	0.016	1.03(13)	1.18(2)	254(1)	4.0(fixed)	254(3)	257(3)
	CT	0.910(2)	4.61	0.007	0.67(12)	0.99(2)	171(1)	6.6(0.3)	176(3)	203(14)
	CG	0.927(2)	4.72	-0.068	0.74(11)	1.08(2)	194(2)	6.1(0.5)	–	–
	CZ	0.867(1)	4.26	-0.038	0.53 (5)	0.94(1)	154(1)	5.9(0.3)	–	–

Notes: standard deviations of $^{VIII}t_{obs}$, M_A/M_B, and $BVsum_{obs}/BVsum_{id}$ calculated by means of error propagation on mean bond distances listed in Table 2. Data in grey are derived from cif files in the ICSD database, and elaborated by means of EosFit7 GUI [63]. Polyhedral bulk moduli of compound YT are derived by calculating volumetric data personally communicated by I. Loa.

3. Octahedral tilting and lattice distortion – first evidence of a dichotomy

The rationalization of perovskite structures in terms of octahedral tilting and polyhedral volume ratios has been studied since the second half of the last century [e.g. 7-9,56-62].

One of the founding concepts of these rationalizations is the Goldschmidt tolerance factor, t. Originally based on the sum of ideal ionic radii, this parameter became more effective in its modified form by Sasaki et al. [6]. Known-as the observed tolerance factor (t_{obs}) since it is calculated on observed bond lengths, this latter parameter is defined as:

$$t_{obs} = \langle A–O \rangle / \sqrt{2}\, \langle B–O \rangle \quad (1)$$

where ⟨A–O⟩ and ⟨B–O⟩ are the mean cation–oxygen distances, with A and B cations 12- (or 8-) and 6-fold coordinated, respectively (values reported in Table 3 and plotted in Figure 1a are calculated by averaging the first eight A–O bond distances, $^{VIII}t_{obs}$).

Later on, Thomas [58] proposed a parameterization where the polyhedral volume ratio (V_A/V_B) of orthorhombic perovskites is determined by tilt angles (θ_x, θ_y, and θ_z) subtended by stalks, defined as lines joining pairs of opposite octahedral vertices, with pseudocubic cell axes, i.e.:

$$V_A/V_B = 6 \cos^2[(\theta_x + \theta_y)/2] \times \cos\theta_z - 1. \quad (2)$$

Regardless of the approach used, Figure 1 shows unequivocally that both parameterizations are strictly related to the mean octahedral bond angle, ⟨B–O–B⟩, which is a sort of average degree of tilting derived from the two symmetry-independent bond angles B–O1–B and B–O2–B.

Accepted manuscript

ACCEPTED MANUSCRIPT

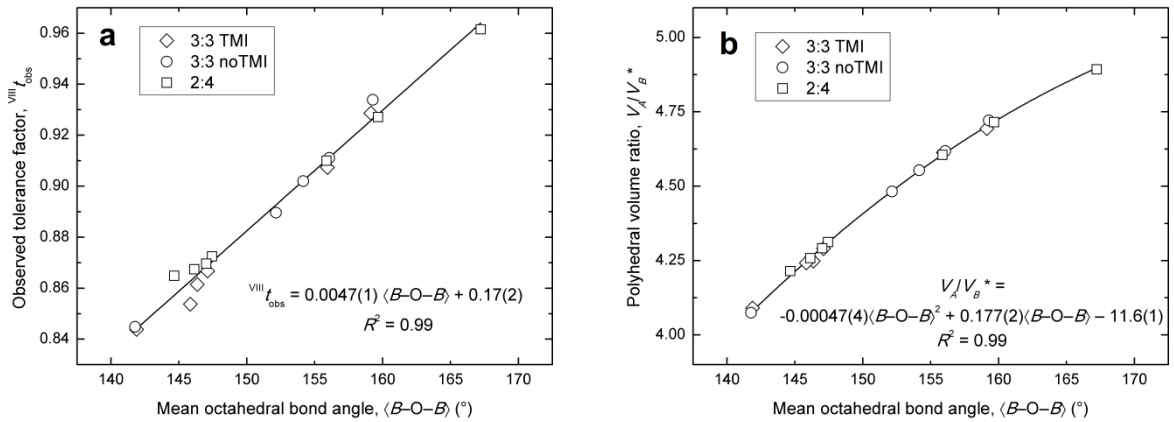

Figure 1 - Observed tolerance factor (a) and polyhedral volume ratio (b), calculated as in Equations 1 and 2, as a function of the average degree of tilting (i.e. ⟨B–O–B⟩). Symbols represent data reported in Tables 2 and 3. Continuous lines represent a linear regression (a) and a second-order polynomial (b) of the plotted data, respectively.

Another useful tool to evaluate the departure of an orthorhombic perovskite from the cubic archetype is the cell distortion factor, d. [6]. Introduced by Sasaki and co-authors, it is calculated by comparing unit-cell axes through the relation $a \approx b \approx \sqrt{2}a_p$, and $c \approx 2a_p$ (in the Pbnm s.g. setting, where $a < b < c$). This factor is defined as:

$$d = [(a/\sqrt{2} - a_p)^2 + (b/\sqrt{2} - a_p)^2 + (c/2 - a_p)^2] / 3a_p^2 \times 10^4 \quad (3)$$

where a_p is the pseudocubic subcell parameter defined as:

$$a_p = (a/\sqrt{2} + b/\sqrt{2} + c/2) / 3. \quad (4)$$

An extended version of Equation 3 has recently been implemented in order to compare the lattice evolution of orthorhombic perovskites under pressure [35,36]. Known-as $d_{norm}(P)$, this parameter defines the rate of change of the cell distortion factor with pressure normalized to the value at ambient conditions (d_0), such as:

$$d_{norm}(P) = 1/d_0 \, (\partial d/\partial P)_T. \quad (5)$$

Once contrasted with unit-cell volume at ambient conditions, the "normalized cell distortion factor with pressure", $d_{norm}(P)$, exhibits distinct trends depending on the chemistry of the perovskite oxide investigated. According to what is stated in the literature (see section 4), Figure 2 highlights qualitatively a dichotomy between perovskites 3:3 and 2:4. Hence, compounds having ions with the same valence at both A and B sites describe trends characterized by small variations in terms of unit-cell volume associated with a significant variation in $d_{norm}(P)$ values. Vice-versa, compounds hosting divalent and tetravalent ions at A and B sites, respectively, cover a volumetric range of about 160 Å^3 (i.e. from compound MS to SC) with a very slight variation in $d_{norm}(P)$ values.
In addition, the two sub-parallel vertical paths (highlighted by dashed lines in Figure 2) suggest a dualism in the behaviour of perovskites 3:3 whether TMI are hosted or not at the octahedral site. Such behaviour, which has never been highlighted before, provides a new perspective into the structural evolution of perovskite compounds under pressure.

Accepted manuscript

ACCEPTED MANUSCRIPT

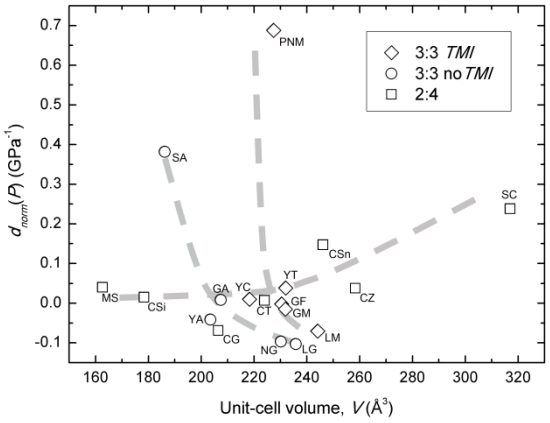

Figure 2 - Normalized cell distortion factor with pressure, $d_{norm}(P)$, as a function of unit-cell volume, V, at ambient conditions. Symbols represent data reported in Tables 2 and 3. Dashed lines are a reader's guide.

4. High-pressure behaviour – reinterpreting a model

As briefly illustrated in the introduction, the pressure-induced evolution of an orthorhombic perovskite can be rationalized in terms of its relative polyhedral compressibility. Models based on this assumption can benefit from the observations raised in the preceding section, i.e.: (1) octahedral tilting in orthorhombic perovskites can be well-approximated using the mean octahedral bond angle, ⟨B–O–B⟩ (Figure 1), and (2) the structural evolution of orthorhombic perovskites with pressure outlines different patterns depending on the formal charge of the cations at cubic and octahedral sites (i.e. whether the perovskite is a 2:4 or a 3:3) and as a result of TMI at the octahedral site (Figure 2).

In the literature, the most comprehensive description of orthorhombic perovskite oxides under high-pressure is that by Zhao et al. [17]. Using this model, the polyhedral compressibility ratio (β_B/β_A) can be devised as the ratio of the estimated bond-valence variation at A and B polyhedral sites due to changes in the average metal–oxygen bond distances. Specifically, this study introduces a site parameter, M_i, defined in terms of the coordination number, N_i, the average metal–oxygen bond distance at A and B site at ambient conditions, R_i, and the bond-valence parameters [64], R_0 and B, where:

$$M_i = (R_i N_i/B) \exp[(R_0 - R_i)/B]. \quad (6)$$

The formulation of this model is consistent with the considerations which were recapped at the beginning of this section. In fact, it entails a dichotomy in the behaviour of perovskite structures under compression. On the basis of the formal charges of the two cations hosted at the cubic and octahedral sites, Zhao and co-workers stated that for perovskites with a formal charge of 2+ at the A site and 4+ at the B site, the compressibility polyhedral ratio $\beta_B/\beta_A = M_A/M_B < 1$, i.e. 2:4 perovskites, will become more distorted with pressure. Conversely, 3:3 perovskites, with cations having the same formal charge (i.e. 3+) at both A and B sites, present a ratio $\beta_B/\beta_A = M_A/M_B > 1$. These latter perovskites are predicted to become less distorted with pressure [17-20].

Although the degree of distortion of each compound cannot be quantified, data in Figure 3a explicitly illustrate dichotomous trends in 2:4 and 3:3 perovskites. In fact, with the exception of the compound PNM, which lies as an outlier, all the orthorhombic perovskite oxides of Figure 3a meet the requirements of the "bond-valence matching" model by Zhao et al. [17].

On the other hand, it is noteworthy that within the reviewed literature, no mention has been made to the duality of perovskites 3:3 whether hosting TMI at the octahedral site or not. Albeit slightly scattered, data shown in Figure 3b, obtained plotting the site parameter ratio, M_A/M_B, as a function of volumetric bulk modulus, K_{T0} (see also data reported in Table 3), further evidence the distinct trends between perovskites 2:4 and 3:3, as well as a splitting originated by TMI within the perovskites 3:3 series.

Accepted manuscript

ACCEPTED MANUSCRIPT

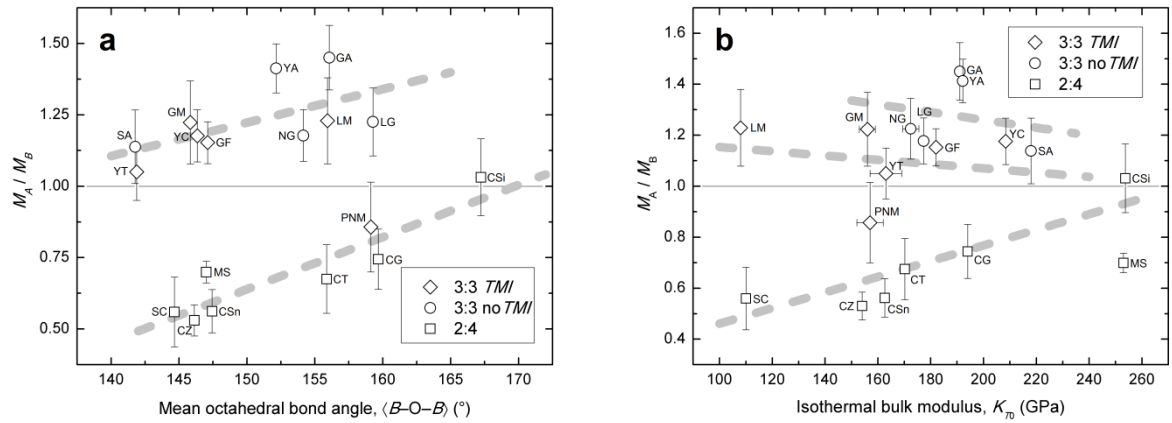

Figure 3 - Ratio of site parameters, M_A/M_B, as defined by Zhao et al. [17] (see text for further details) as a function of (a) average degree of tilting, ⟨B–O–B⟩, and (b) isothermal bulk modulus, K_{T0}. Symbols refer to data in Tables 2 and 3. Dashed lines are a reader's guide.

As well the "bond-valence matching" model by Zhao et al. [17], the "polyhedral bond-valence ratio" [29,30] is another approach which makes use of Brown's bond-valence method [64]. Developed to evaluate the lattice strain associated with different local arrangements of ligands at a coordination site, the ratio between the observed bond-valence sum of polyhedra which share oxygens coordinating the octahedral site ($BVsum_{obs}$) with respect to the bond-valence sum calculated from ideal bond distances for each polyhedron ($BVsum_{id}$) has been demonstrated to scale linearly with the local bond distances at octahedral and tetrahedral sites of several silicates and oxides (an example is reported in [29]). Furthermore, the latter approach has been proposed as an effective tool when used to compare structures with similar atomic packing, e.g. in dense structures, along isomorphic solid solutions and structures with the same lattice topology [29,30].
In Figure 4, data calculated using Equation 6 (i.e. the bond-valence matching model) are plotted as a function of those obtained using the polyhedral bond-valence ratio (see also Table 3). As clearly shown in this figure, each dataset of orthorhombic perovskites outlines a distinct path emphasizing that the chemistry of these compounds rules the dynamics of distortion and compressibility.
In addition, it can be noted that for most of the perovskite compounds under comparison, local distances at the octahedral site and the polyhedra which coordinate it are somehow "balanced" (i.e. $BVsum_{obs}/BVsum_{id}$ ranges from 0.95 to 1.05). In point of fact, only the compound CSi and, to a lesser extent, CG possess observed bond-distances in polyhedra coordinating the octahedral site which are shorter than ideal, meaning that the oxygens shared to the octahedral site are pulled towards the second nearest neighbouring polyhedra ($BVsum_{obs}/BVsum_{id} > 1$). Vice versa, only the compound SC has a $BVsum_{obs}/BVsum_{id}$ ratio significantly smaller than 1. In this case, cations located in the second nearest neighbouring polyhedra with respect to the octahedral site are relatively underbonded since the observed bond distances are longer than the ideal values adopted using the bond-valence method.

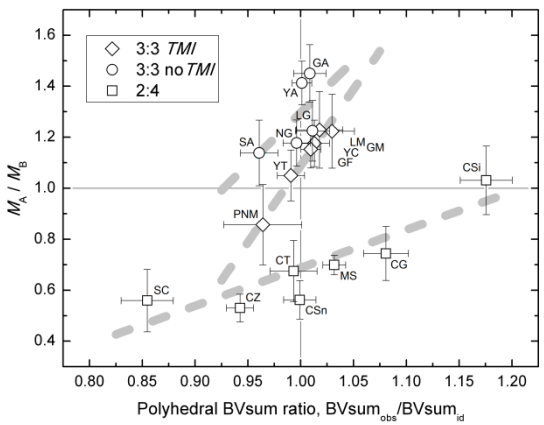

ACCEPTED MANUSCRIPT

Figure 4 - Polyhedral bond-valence sum ratio [29,30] vs. ratio of site parameters M_A/M_B [17]. Dashed lines are a reader's guide. An example of calculating the "polyhedral bond-valence sum ratio" is given in [29].

Therefore, on the basis of the effects detected with TMI, all previous approaches in predicting the structural evolution and polyhedral compressibility of orthorhombic perovskites should be reconsidered.

5. Octahedral tilting spread

Considering that the perovskite structure basically consists of a framework of corner-sharing octahedra, in Figure 5 the volume of the octahedral site at ambient pressure, $V(BO_6)$, is contrasted to its isothermal bulk modulus, $K_{P0}(B)$.

Although each perovskite dataset (i.e. 3:3 TMI, 3:3 noTMI, and 2:4 perovskites) outlines a distinct trend, simple correlations between the volume at room pressure and the bulk modulus of B site are impossible, especially for compounds 3:3 TMI. In line with what was previously stated, it can be supposed that perovskite polyhedra compressibility and degree of tilting are related. Even if most orthorhombic perovskites have relatively undistorted octahedra, as previously shown in Figure 1, a very wide degree of octahedral tilting can be exhibited. For example, in the case of the selected compounds, ⟨B–O–B⟩ can range from almost untilted $CaSiO_3$ (167°) and $CaGeO_3$ (160°) to extremely tilted $YTiO_3$ and $ScAlO_3$ where ⟨B–O–B⟩ ≈ 142° (see also Table 2).

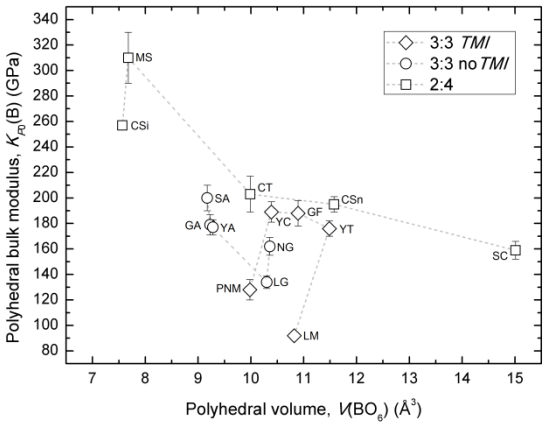

Figure 5 - Polyhedral bulk modulus as a function of polyhedral volume at ambient pressure for the octahedral site in orthorhombic perovskites. Symbols refer to experimental data in Tables 2 and 3.

In order to confirm whether octahedral tilting is responsible or not for the data scatter in Figure 5 and to establish the extent of its spreading, it could be useful to focus on the rest of the perovskite lattice, i.e. on cubic polyhedron. Since cubic sites in a perovskite structure are located within the network of corner-sharing octahedra, it follows that the distortion of AO_{12} polyhedra mainly derives from the tilting of the octahedral framework (Figure 6a). According to Zhao et al. [17], the contribution of the bond distances between atom A and its 12 coordinated anions can be split into two parts. Specifically, a separate contribution of the changes in the average of the eight shorter A–O distances and the four longer A–O distances at the cubic site has been considered (Figures 6b and 6c).

ACCEPTED MANUSCRIPT

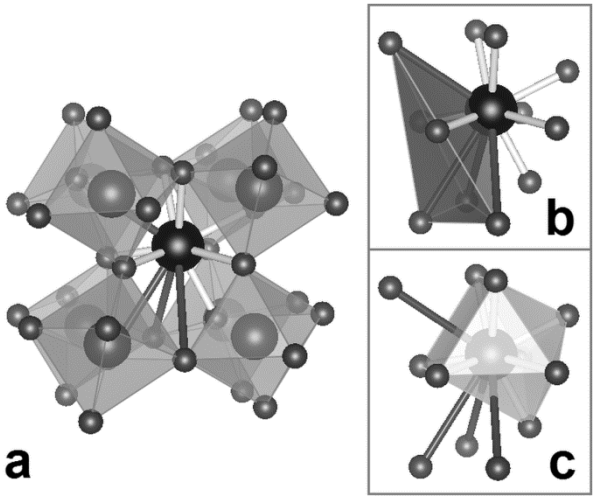

Figure 6 - Schematic illustration of the twelve-coordinated cubic site of $ScAlO_3$ perovskite (compound SA) at room pressure obtained using the VESTA v.3.2.1 visualizer [65]. The longer four A–O bond distances are those in dark grey (a-c). Furthermore, the volume due to the contribution of the average of the four longer A–O distances, V_{AO4} (b) and the eight shorter A–O distances, V_{AO8} (c) are highlighted in two separate boxes.

Zhao and co-authors asserted that the four longer A–O distances are strongly related to the amount of distortion in the AO_{12} site [17]. This is particularly evident for those compounds characterized by octahedral sites occupied by TMI (Figure 7).
When contrasted with polyhedral volume, A site bulk modulus can be well-approximated using linear trends for compounds labelled 2:4 and 3:3 noTMI (Figure 7a), while the contribution of the four longer A–O distances at the cubic site (see Figure 6b) returns no physically reasonable correlations for perovskite structures hosting TMI at the octahedral site. The details of cubic compressibility with respect to V_{AO4} in Figure 7b reveal a high data scatter, meaning that the four longer A–O bond distances in a perovskite structure can be strongly affected by polyhedral distortion.

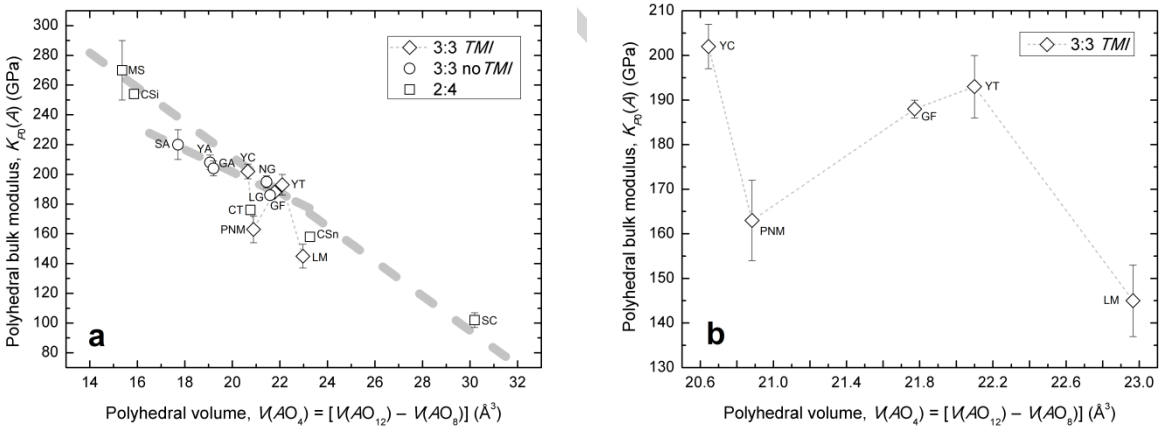

Figure 7 - Polyhedral bulk modulus as a function of polyhedral volume due to the contribution of the average of the four longer A–O distances at the cubic site of orthorhombic perovskites (a); and (b) detail of the evolution of the cubic bulk modulus of perovskites 3:3 with TMI. Symbols refer to experimental data in Tables 2 and 3. Thick dashed lines in (a) are a reader's guide.

Clearly, it can now be considered that the octahedral tilting of an orthorhombic perovskite induces a distortion which spreads up to the second shell, i.e. to longer cubic bond distances, where the distortion seems to be confined.

6. Predicting polyhedral compressibility

ACCEPTED MANUSCRIPT

In line with the main purpose of high-pressure models, it would seem extremely advantageous to obtain solid relationships between volume at ambient pressure and the isothermal bulk modulus of perovskite polyhedra. Therefore, this last section is aimed at identifying new relationships to enable the behaviour of orthorhombic perovskites at high-pressure to be predicted using a combined analysis of experimental data at both ambient and high-pressure.

In Figure 8, the isothermal bulk modulus of the cubic site of orthorhombic perovskites, $K_{P0}(A)$, is plotted versus the polyhedral volume calculated on the eight shorter A–O bond distances at ambient pressure, V_{AO8} (see Figure 6c). Although characterized by a limited amount of data, i.e. five samples for each dataset, each trend describes a linear relationship which entails two important implications. Firstly, on the basis of perovskite chemical composition (i.e. 2:4, 3:3 TMI, and 3:3 noTMI), A-site compressibility can be obtained using polyhedral volume at the cubic site at ambient conditions with a good degree of accuracy (see equations and the respective agreement factors for the linear fit of data in Figure 8). Secondly, the distortion effects induced by octahedral tilting are extremely limited or absent within the first shell of A-site (i.e. as previously suggested, cubic site distortion is mainly accommodated by the four longer cubic bond distances).

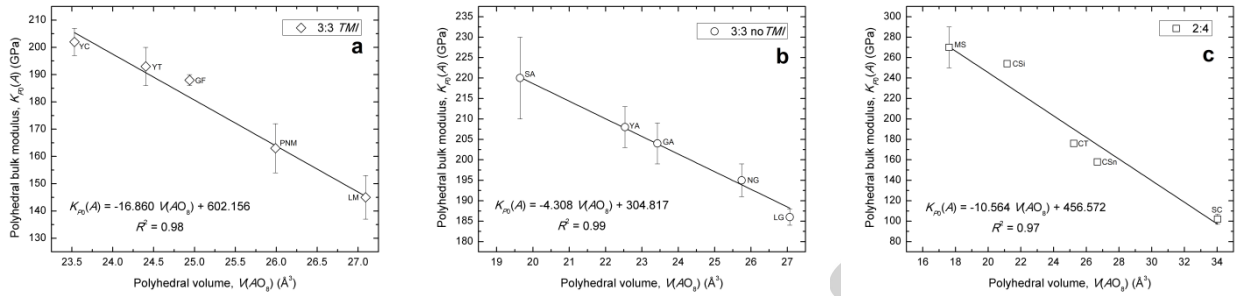

Figure 8 - AO_8 polyhedral volume versus polyhedral bulk modulus, $K_{P0}(A)$, in orthorhombic perovskites. Symbols refer to experimental data in Tables 2 and 3. Solid lines result from a linear fit of the data.

In an iterative but likewise effective manner, the relationships shown in Figure 9 demonstrate that, as well as for those linking distortion and tilting, the driving forces ruling the polyhedral compressibility of cubic and octahedral sites are strictly interconnected.

Indeed, once matched to each other, the polyhedral bulk moduli of A and B sites can be related using linear functions (i.e. solid lines in Figure 9).

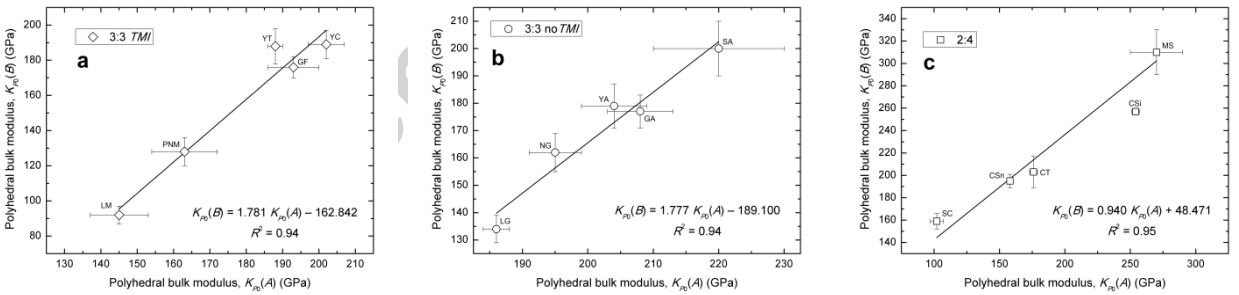

Figure 9 - Cubic, $K_{P0}(A)$, versus octahedral, $K_{P0}(B)$, bulk modulus in orthorhombic perovskites. Symbols refer to experimental data in Table 3. Solid lines result from a linear fit of the data.

Equations derived from linear regressions in Figure 9, as well as those in Figure 8, can be expressed as variations of cubic polyhedral volume $V(AO_8)$. This means the ratio of the compressibility of A and B polyhedral sites can be expressed as a univocal function of $V(AO_8)$ using the following equations:

3:3 TMI: $$\frac{K_{P0(A)}}{K_{P0(B)}} = \frac{20.0491 - 0.5614 \cdot V(AO_8)}{30.2931 - V(AO_8)}; \quad (1)$$

3:3 noTMI: $$\frac{K_{P0(A)}}{K_{P0(B)}} = \frac{39.8126 - 0.5627 \cdot V(AO_8)}{46.0496 - V(AO_8)}; \quad (2)$$

ACCEPTED MANUSCRIPT

2:4: $$\frac{K_{P0(A)}}{K_{P0(B)}} = \frac{45.9442 - 1.0636 \cdot V(AO_8)}{48.073 - V(AO_8)}. \quad (3)$$

From a merely mathematical point of view, the polyhedral compressibility ratio $K_{P0}(A)$ / $K_{P0}(B)$ calculated over discrete steps of $V(AO_8)$ gives rise to an injective function in the positive real (note: in order to maintain the physical meaning of V and K_{P0}, $V(AO_8)$, $K_{P0}(A)$, and $K_{P0}(B)$ are greater than 0). Irrespective of the chemical nature of A and B cations, the graph of the resulting functions is the set of curvilinear patterns (grey symbols) shown in Figure 10.

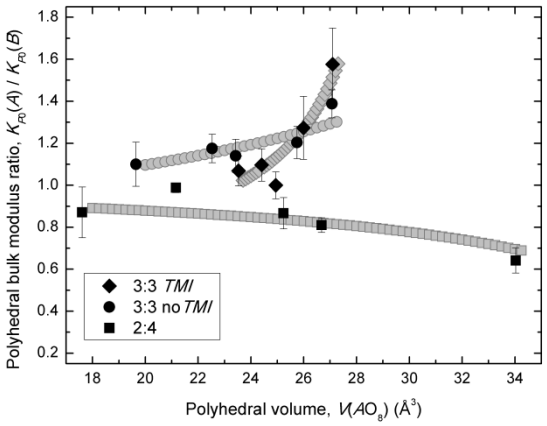

Figure 10 - Polyhedral bulk modulus ratio $K_{P0}(A)$ / $K_{P0}(B)$ as a function of a discrete variation of cubic polyhedral volume, $V(AO_8)$. Selected orthorhombic perovskites (experimental data) are in black.

The trend of these theoretical patterns is perfectly described by a cubic regression of the polyhedral compressibility ratio $K_{P0}(A)$ / $K_{P0}(B)$ on $V(AO_8)$:

3:3 TMI: $$\frac{K_{P0(A)}}{K_{P0(B)}} = 0.0069 \cdot V(AO_8)^3 - 0.4974 \cdot V(AO_8)^2 + 12.0068 \cdot V(AO_8) - 96.236 \quad (4)$$
$R^2 = 0.99$;

3:3 noTMI: $$\frac{K_{P0(A)}}{K_{P0(B)}} = 5.6705 \cdot 10^{-5} \cdot V(AO_8)^3 - 0.0028 \cdot V(AO_8)^2 + 0.0629 \cdot V(AO_8) + 0.4866 \quad (5)$$
$R^2 = 1.00$;

2:4: $$\frac{K_{P0(A)}}{K_{P0(B)}} = -2.6277 \cdot 10^{-5} \cdot V(AO_8)^3 + 0.0015 \cdot V(AO_8)^2 - 0.0354 \cdot V(AO_8) + 1.1961 \quad (6)$$
$R^2 = 0.99$.

A further survey on the compressibility features of the compounds under investigation reveals that the volumetric bulk modulus K_{T0} can also be related to cubic polyhedral volume $V(AO_8)$. As is well shown in Figure 11, with an appreciable degree of confidence, the volumetric bulk modulus of each perovskite series scales linearly with the polyhedral volume calculated on the eight shorter A–O bond distances at ambient pressure.

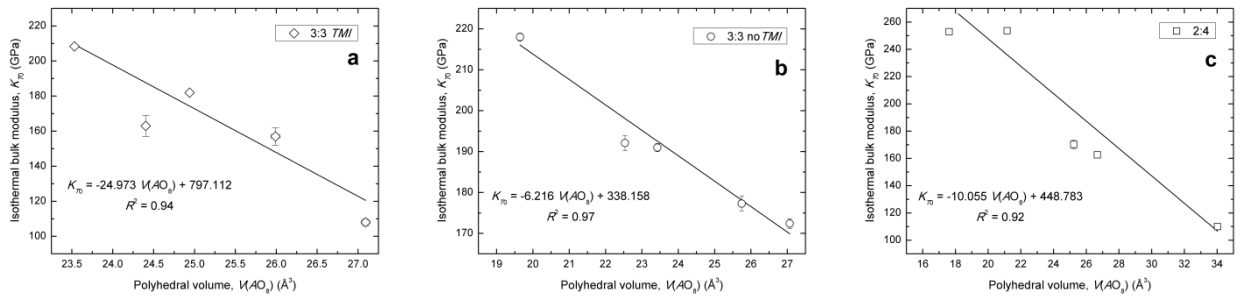

ACCEPTED MANUSCRIPT

Figure 11 - AO_8 polyhedral volume versus volumetric bulk modulus, K_{T0}, in orthorhombic perovskites. Symbols refer to experimental data in Tables 2 and 3. Solid lines result from a linear regression of the data.

By combining the previous set of equations (i.e. 4-6 with those in Figure 11), it is therefore possible to achieve a semiempirical but solid relationship between the ratio of A and B polyhedral site compressibility and the volumetric bulk modulus, K_{T0}, of orthorhombic perovskites (see Figure 12).

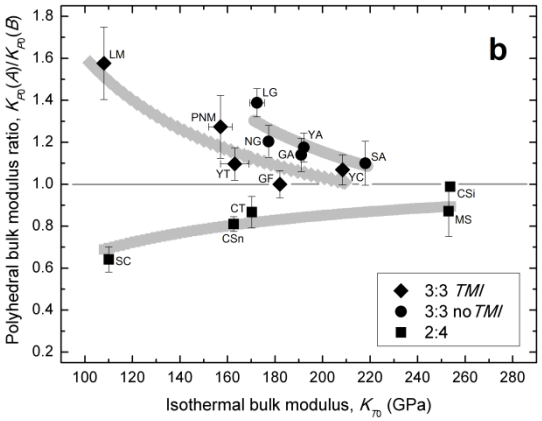

Figure 12 - Polyhedral bulk modulus ratio $K_{P0}(A)$ / $K_{P0}(B)$ as a function of isothermal volumetric bulk modulus function, K_{T0} (black symbols). Patterns in grey are derived by combining equations 4 to 6 with those reported in Figure 11 (see text for further details).

Figure 12 again highlights the threefold behaviour of orthorhombic perovskites with pressure and for the first time in literature provides indications of convergent trends towards the highest values of volumetric bulk moduli, namely the higher the volumetric bulk modulus along each dataset (i.e. 2:4, 3:3 TMI, and 3:3 noTMI perovskites) the closer the compressibility of octahedra and cubic sites.
The combination of equations 4-6 with those reported in Figure 11 gives rise to a set of curvilinear trends (one for each perovskite family) which can be adequately described by fitting to the following polynomial expressions of the second order:

3:3 TMI: $$\frac{K_{P0(A)}}{K_{P0(B)}} = 4.7714 \cdot 10^{-5} \cdot {K_{T0}}^2 - 0.0212 \cdot K_{T0} + 3.3674 \quad (7)$$
$$R^2 = 0.99;$$

3:3 TMI: $$\frac{K_{P0(A)}}{K_{P0(B)}} = 3.1636 \cdot 10^{-5} \cdot {K_{T0}}^2 - 0.0166 \cdot K_{T0} + 3.2079 \quad (8)$$
$$R^2 = 0.99;$$

3:3 TMI: $$\frac{K_{P0(A)}}{K_{P0(B)}} = -5.3527 \cdot 10^{-6} \cdot {K_{T0}}^2 + 0.0032 \cdot K_{T0} + 0.4229 \quad (9)$$
$$R^2 = 0.99.$$

In conclusion, Figure 12 illustrates the empirical relationships identified in Figures 8, 9, and 11, recasted as in Figures 10, which perfectly overlay on each set of experimental data. Although this is an approximation related to a semi-empirical formalism, it can be asserted that the yielded equations can be applied to design a hypothetical perovskite compound with known composition and whose evolution in compression must be predicted.

7. Conclusions

The evolution of orthorhombic perovskites at high-pressure has been reviewed and systematised, focusing particularly on effects deriving from the chemical nature of the cation constituents, especially whether transition metal ions (TMI) are hosted at the octahedral site. The most common parameterizations and models used to classify orthorhombic perovskites and rationalize their behaviour at ambient and high-

Accepted manuscript

ACCEPTED MANUSCRIPT

pressure conditions have been revisited in order to connect octahedral tilting with the compressibility of AO_{12} and BO_6 polyhedra.

Moreover, in order to confirm the common paradigm which states that the evolution of orthorhombic perovskites with pressure defines dichotomous trends depending on the formal charge of A and B cations, it has been shown that perovskites 3:3 define different patterns whether bearing TMI or not.

The behaviour of orthorhombic perovskites at high-pressure as highlighted by this contribution provides new useful constraints both for designing compounds with specific physical properties as well as for determining more accurate models of the Earth's interior.

Acknowledgements

I would like to express my thanks to Giuseppe Cruciani, Michele Dondi and Annalisa Martucci for their discussions and critical readings which have surely enhanced the quality of this contribution. The constructive reviews of three anonymous referees, and specific suggestions by the editor (Prof. A. Bansil) greatly improved this paper.

References

[1] Y. Maeno, H. Hashimoto, K. Yoshida, S. Nishizaki, T. Fujita, J.G. Bednorz, F. Lichtenberg, Nature 372 (1994) 532–534.
[2] M. Jansen, H.P. Letschert, Nature 404 (2000) 980–982.
[3] M. Ye, X. Wen, M. Wang, J. Iocozzia, N. Zhang, C. Lin, Z. Lin, Mater. Today 18 (2015) 155–162.
[4] F. Deschler, M. Price, S. Pathak, L.E. Klintberg, D.D. Jarausch, R. Higler, S. Hüttner, T. Leijtens, S.D. Stranks, H.J. Snaith, M. Atatüre, R.T. Phillips, R.H. Friend, J. Phys. Chem. Lett. 5 (2014) 1421–1426.
[5] R.H. Mitchell, Perovskites: Modern and ancient, Almaz Press, Ontario, 2002.
[6] S. Sasaki, C.T. Prewitt, R.C. Liebermann, Am. Mineral. 68 (1983) 1189–1198.
[7] A.M. Glazer, Acta Crystallogr. B 28 (1972) 3384–3392.
[8] P.M. Woodward, Acta Crystallogr. B 53 (1997) 32–43.
[9] M. Avdeev, E.N. Caspi, S. Yakovlev, Acta Crystallogr. B 63 (2007) 363–372.
[10] T. Duffy, Nature 506 (2014) 427–429.
[11] E. Knittle, R. Jeanloz, G.L. Smith, Nature 319 (1986) 214–216.
[12] A. Navrotsky, D.J. Weidner, Perovskite: a structure of great interest to geophysics and materials science, American Geophysical Union, 1989.
[13] M. Murakami, K. Hirose, K. Kawamura, N. Sata, Y. Ohishi, Science 304 (2004) 855–858.
[14] A.R. Oganov, S. Ono, Nature 430 (2004) 445–448.
[15] D. Andrault, J.P. Poirier, Phys. Chem. Minerals 18 (1991) 91–105.
[16] N.W. Thomas, Acta Crystallogr. B 54 (1998) 585–599.
[17] J. Zhao, N.L. Ross, R.J. Angel, Acta Crystallogr. B 60 (2004) 263–271.
[18] R.J. Angel, N.L. Ross, J. Zhao, Eur. J. Mineral. 17 (2005) 193–199.
[19] R.J. Angel, J. Zhao, N.L. Ross, Phys. Rev. Lett. 95 (2005) 025503.
[20] J. Zhao, N.L. Ross, R.J. Angel, Acta Crystallogr. B 62 (2006) 431–439.
[21] T. Yagi, H.-K. Mao, P.M. Bell, Phys. Chem. Minerals 3 (1978) 97–110.
[22] M. O'Keeffe, B.G. Hyde, J.-O. Bovin, Phys. Chem. Minerals 4 (1979) 299–305.
[23] D.P. Kozlenko, B. Savenko, Phys. Part. Nuclei 37 (2006) 1–12.
[24] J.B. Goodenough, J. Zhou, J. Mater. Chem. 17 (2007) 2394–2405.
[25] D. Bizen, K. Nakatsuka, T. Murata, H. Nakao, Y. Murakami, Phys. Rev. B 78 (2008) 224104.
[26] I.S. Lyubutin, A.G. Gavriliuk, Phys.–Uspekhi 52 (2009) 989–1017.
[27] F. Aguado, F. Rodríguez, R. Valiente, J.-P. Itiè, M. Hanfland, Phys. Rev. B 85 (2012) 100101.
[28] K. Catalli, S.-H. Shim, P. Dera, V.B. Prakapenka, J. Zhao, W. Sturhahn, P. Chow, Y. Xiao, H. Cynn, W.J. Evans, Earth Planet. Sc. Lett. 310 (2011) 293–302.
[29] M. Ardit, M. Dondi, C. Zanelli, G. Cruciani, Z. Kristallogr. 229 (2014) 687–697.
[30] M. Dondi, M. Ardit, G. Cruciani, C. Zanelli, Am. Mineral. 99 (2014) 1736–1745.
[31] D.P. Kozlenko, Z. Jirak, I.N. Goncharenko, B.N. Savenko, J. Phys.-Condens. Mat. 16 (2004) 5883–5895.
[32] J.R. Hester, K. Tomimoto, H. Noma, F.P. Okamura, J. Akimitsu, Acta Crystallogr. B 53 (1997) 739–744.

Accepted manuscript

ACCEPTED MANUSCRIPT

[33] I. Loa, X. Wang, K. Syassen, H. Roth, T. Lorenz, M. Hanfland, Y.L. Mathis, J. Phys.-Condens. Mat. 19 (2007) 406223.
[34] G. Cruciani, M. Ardit, M. Dondi, F. Matteucci, M. Blosi, M.C. Dalconi, S. Albonetti, J. Phys. Chem. A 113 (2009) 13772–13778.
[35] M. Ardit, G. Cruciani, M. Dondi, M. Merlini, P. Bouvier, Phys. Rev. B 82 (2010) 064109.
[36] M. Ardit, M. Dondi, G. Cruciani, in: S.V. Krivovichev (Ed.), Minerals as Advanced Materials II, Springer, Berlin, 2012, pp. 305–318.
[37] N.L. Ross, J. Zhao, R.J. Angel, J. Solid State Chem. 177 (2004) 3768–3775.
[38] P. Norby, I.G. Krogh Andersen, E. Krogh Andersen, J. Solid State Chem. 119 (1995) 191–196.
[39] I. Loa, P. Adler, A. Grzechnik, K. Syassen, U. Schwarz, M. Hanfland, G.Kh. Rozenberg, P. Gorodetsky, M.P. Pasternak, Phys. Rev. Lett. 87 (2001) 125501.
[40] T. Mori, N. Kamegashira, K. Aoki, T. Shishido, T. Fukuda, Mater. Lett. 54 (2002) 238–243.
[41] C. Lin, Y. Zhang, J. Liu, X. Li, Y. Li, L. Tang, L. Xiong, J. Phys.-Condens. Mat. 24 (2012) 115402.
[42] N.L. Ross, Phys. Chem. Minerals 25 (1998) 597–602.
[43] N.L. Ross, J. Zhao, R.J. Angel, J. Solid State Chem. 177 (2004) 1276–1284.
[44] R.J. Angel, J. Zhao, N.L. Ross, C.V. Jakeways, S.A.T. Redfern, M. Berkowski, J. Solid State Chem. 180 (2007) 3408–3424.
[45] A. Saiki, Y. Seto, H. Seki, N. Ishizawa, M. Kato, N. Mizutani, Nippon Kagaku Kaishi (1991) 25–31.
[46] K.S. Knight, W.G. Marshall, N. Bonanos, D.J. Francis, J. Alloy. Compd. 394 (2005) 131–137.
[47] J. Zhao, N.L. Ross, R.J. Angel, Phys. Chem. Minerals 31 (2004) 299–305.
[48] J. Kung, R.J. Angel, N.L. Ross, Phys. Chem. Minerals 28 (2001) 35–43.
[49] M. Sugahara, A. Yoshiasa, Y. Komatsu, T. Yamanaka, N. Bolfan-Casanova, A. Nakatsuka, S. Sasaki, M. Tanaka, Am. Mineral. 91 (2006) 533–536.
[50] C.B. Vanpeteghem, J. Zhao, R.J. Angel, N.L. Ross, N. Bolfan-Casanova, Geophys. Res. Lett. 33 (2006) L03306.
[51] R. Caracas, R.M. Wentzcovitch, Acta Crystallogr. B. 62 (2006) 1025–1030.
[52] J. Zhao, N.L. Ross, D. Wang, R.J. Angel, J. Phys.-Condens. Mat. 23 (2011) 455401.
[53] N.L. Ross, R.J. Angel, Am. Mineral. 84 (1999) 277–281.
[54] H.J.A. Koopmans, G.M.H. van de Velde, P.J. Gellings, Acta Crystallogr. C 39 (1983) 1323–1325.
[55] N.L. Ross, T.D. Chaplin, J. Solid State Chem. 172 (2003) 123–126.
[56] A.M. Glazer, Acta Crystallogr. A 31 (1975) 756–762.
[57] N.W. Thomas, Acta Crystallogr. B 45 (1989) 337–344.
[58] N.W. Thomas, Acta Crystallogr. B 52 (1996) 16–31.
[59] C.J. Howard, H.T. Stokes, Acta Crystallogr. B 54 (1998) 782–789.
[60] C.J. Howard, H.T. Stokes, Acta Crystallogr. B 60 (2004) 674–684.
[61] C.J. Howard, H.T. Stokes, Acta Crystallogr. A 61 (2005) 93–111.
[62] D. Wang, R.J. Angel, Acta Crystallogr. B 67 (2011) 302–314.
[63] R.J. Angel, J. Gonzalez-Platas, M. Alvaro, Z. Kristallogr. 229 (2014) 405–419.
[64] I.D. Brown, The chemical bond in inorganic chemistry. The bond valence model, IUCr monograph on crystallography, Oxford University Press, Oxford, 2002.
[65] K. Momma, F. Izumi, J. Appl. Crystallogr. 44 (2011) 1272–1276.

Accepted manuscript

Graphical abstract

ACCEPTED MANUSCRIPT

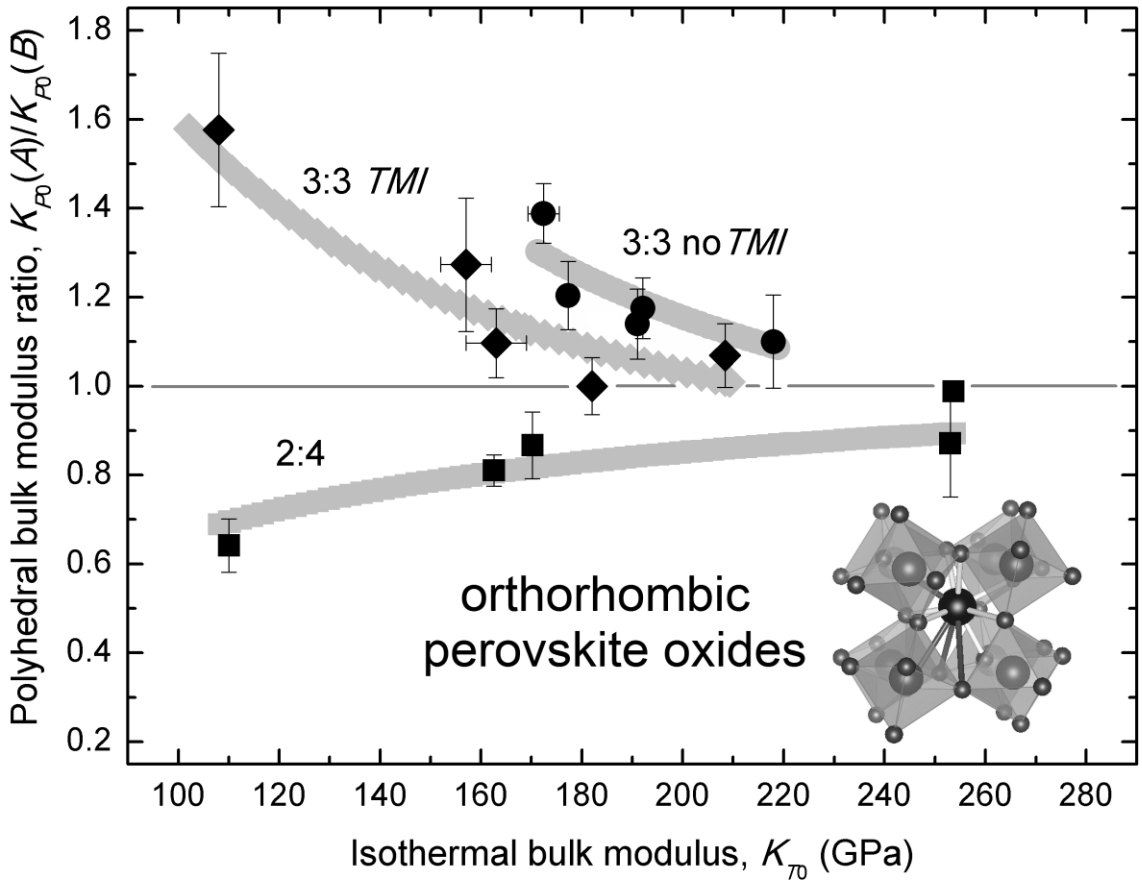

Highlights

- overview of the high-pressure evolution of ABO_3 orthorhombic perovskites;
- review of several models to systematise the behaviour of these compounds at HP;
- constant evidence of a dichotomy between $A^{2+}B^{4+}O_3$ and $A^{3+}B^{3+}O_3$ perovskites;
- systematic dualism in $A^{3+}B^{3+}O_3$ if transition metal ions are hosted at B site;
- new perspective on the pressure-induced distortion of orthorhombic perovskites.

Accepted m